

# Study of the Viscosity of Mold Flux Based on the Vogel–Fulcher–Tammann (VFT) Model



LEJUN ZHOU and WANLIN WANG

Viscosity is one of the most important properties of mold flux and affects the process of continuous casting significantly. In order to describe the variation of viscosity of mold flux accurately in a wide range of temperature occurring in the casting mold, a non-Arrhenius Vogel–Fulcher–Tammann (VFT) model was adopted in this study. The results showed that the adjusted coefficient of determination (Adj.  $R^2$ ) of non-Arrhenius VFT Model ranges from 0.92 to 0.96, which suggests this model could be well adapted to predict the relationship between viscosity and temperature of mold flux. The temperature at which viscosity becomes infinite,  $T_{VFT}$ , increased with the addition of  $Cr_2O_3$  and improvement of basicity, while it decreased with the addition of  $B_2O_3$ , as it was determined by both the degree of polymerization of the melt structure and crystallization behavior of the melt. Also, the pseudo-activation energy,  $E_{VFT}$ , of Samples 1 to 5 was  $60.1 \pm 3.6$ ,  $94.7 \pm 14.9$ ,  $101.7 \pm 19.0$ ,  $38.0 \pm 4.8$ , and  $32.4 \pm 4.0$  kJ/mol, respectively; it increased with the addition of  $Cr_2O_3$  and  $B_2O_3$ , but decreased with the increase of basicity.

DOI: 10.1007/s11663-016-0835-2

© The Minerals, Metals & Materials Society and ASM International 2016

## I. INTRODUCTION

THE mold flux plays important roles in the process of continuous casting, such as the lubrication of shell during the mold oscillation, in-mold heat transfer control, and adsorption of inclusions on top of molten steel, which are greatly influenced by the viscosity of mold flux. Mold flux with improper viscosity would cause lots of problems, for example, the presence of severe oscillation marks, surface cracks, breakouts,<sup>[1,2]</sup> the entrapment of slag on top of molten steel,<sup>[3]</sup> the erosion of the nozzle in the slag layer,<sup>[4]</sup> and the formation of large slag rim in the vicinity of meniscus.<sup>[5]</sup> Therefore, it is significantly important to describe the viscosity of mold flux accurately during the process of continuous casting.

A variety of approaches and models have been used to describe the viscosity of liquid mold flux as a function of temperature and chemical composition. Among them, the temperature-dependent viscosity models include empirical,<sup>[6]</sup> Arrhenius,<sup>[7,8]</sup> and Weymann–Frenkel model,<sup>[9]</sup> while the composition-dependent viscosity models include quasi-structural,<sup>[10]</sup> basicity index,<sup>[11,12]</sup> and optical basicity model.<sup>[13,14]</sup> However, most of those models are limited to a relatively small range of temperature and viscosity. The mold flux in continuous

casting mold experiences a wide temperature gradient ranging from more than 1773 K (1500 °C) to room temperature; as the temperature of liquid mold flux is close to the molten steel when it contacts with molten steel; while the temperature decreases to the break temperature after it infiltrates into the gap between mold wall and shell; and then it further decreases to room temperature when the mold flux exists out with the slab from the bottom of mold. Thus, the viscosity of mold flux shows a strong function of temperature.

The Vogel–Fulcher–Tammann (VFT) model was proposed independently by Vogel (in 1921), Fulcher (in 1925), and Tammann (in 1926),<sup>[15–17]</sup> which is one of the most widely used non-Arrhenius temperature-dependent viscosity model. The VFT relation has been found to be a good prediction model for many classes of materials, and has been cited in hundreds of articles. For example, Giordano, *et al.*<sup>[18,19]</sup> used the VFT model to study the rheology of magma. Research works from Angel, *et al.*<sup>[20]</sup> suggested that the viscosity of glassy alloys shows perfect VFT equation behavior. Lu, *et al.*<sup>[21]</sup> found that the VFT model was able to provide an accurate prediction for the temperature-dependent relaxation behavior of shape-memory polymers. Mokhtarani, *et al.*<sup>[22]</sup> also successfully fitted the experimental viscosity of pure and binary ionic liquids using the VFT viscosity model.

Although the VFT model has been widely used to characterize the viscosity of many materials, it has never been adopted to study the rheological property of mold flux. Therefore, in this paper, the viscosity of mold fluxes at the temperature ranging from 1200 K (927 °C) to 1573 K (1300 °C) was measured firstly; then, the relationship between viscosity and temperature was analyzed by both Arrhenius model and non-Arrhenius

LEJUN ZHOU, Lecturer, is with the School of Metallurgy and Environment, Central South University, Changsha, 410083, P.R. China. WANLIN WANG, Lotus Professor, is with the School of Metallurgy and Environment, and also Director of National Center for International Research of Clean Metallurgy, Central South University, Changsha P.R. China. Contact e-mail: wanlin.wang@gmail.com

Manuscript submitted May 23, 2016.

Article published online October 17, 2016.

VFT model; finally, the effects of mold flux components on the VFT temperature and pseudo-activation energy were also discussed.

## II. EXPERIMENT METHOD

### A. The Raw Materials

The designed mold fluxes in this study are listed in Table I. Among them, Sample 1 is a decarburized commercial mold flux for the casting of low-carbon steel by placing it into a programmable furnace at 1073 K (800 °C) for 24 hours. Samples 2 to 5 were prepared by adding different amount of reagent grade chemicals of CaCO<sub>3</sub>, SiO<sub>2</sub>, Al<sub>2</sub>O<sub>3</sub>, MnCO<sub>3</sub>, Na<sub>2</sub>CO<sub>3</sub>, Li<sub>2</sub>CO<sub>3</sub>, CaF<sub>2</sub>, Cr<sub>2</sub>O<sub>3</sub>, and B<sub>2</sub>O<sub>3</sub> (Supplier: Fine chemical engineering and technology research and development center, Guangdong, China) into Sample 1 to adjust their compositions. All samples were stirred in a blender for 120 minutes to homogenize their compositions before the viscosity test.

### B. Experiment Apparatus and Process

The viscosity measurements were carried out using a Brookfield DV-II+ viscometer (Brookfield Inc.) through the rotating cylinder method, which is schematically shown in Figure 1. A calibration measurement was carried out at room temperature using stand oil with known viscosity.<sup>[23]</sup>

When measuring the viscosity of the designed mold flux, 250 g of the sample powders was firstly placed in a graphite crucible with a diameter and an internal height of 50 and 80 mm, respectively (Table II). Second, the crucible was heated to 1773 K (1500 °C) and held for 10 minutes to obtain a homogeneous melt in an electric resistance furnace with MoSi<sub>2</sub> as the heating element. Then, the melt was cooled to the target temperature. After that, a bob, which is made of molybdenum with the height of 18 mm and the diameter of 15 mm (Table II), was immersed into liquid slag bath and rotated to obtain the value of viscosity at the target temperature.

The composition of mold fluxes after viscosity measurement tests was also analyzed by the X-ray fluorescence (XRF, S4Pioneer; Bruker AXS; GmbH Karlsruhe, Germany) and inductively coupled plasma mass spectrometry (ICP, SPECTRO, Germany). The results are shown in Table III. It could be found that the evaporative loss of mold flux components is relatively

small, and the influence caused by the evaporation can be ignored, which is consistent with our previous study.<sup>[24]</sup>

In order to investigate the precipitated phase of mold fluxes after the viscosity tests, parts of mold fluxes after the viscosity measurements at the target temperature of 1573 K (1300 °C) were obtained by a molybdenum spoon and quenched in water. Then, those quenched mold fluxes were sampled and observed through scanning electron microscope (Japanese Electronics Company JSM-6360LV) with an acceleration voltage of 20 kW and 200 times magnification.

### C. The Vogel–Fulcher–Tammann (VFT) Non-Arrhenius Model

The generic relation for the Vogel–Fulcher–Tammann (VFT) model is as following:

$$\log \eta = A_{\text{VFT}} + \frac{E_{\text{VFT}}}{T - T_{\text{VFT}}}, \quad [1]$$

where,  $\eta$  (Pa·s) is the viscosity of mold flux, and the adjustable parameters  $A_{\text{VFT}}$ ,  $E_{\text{VFT}}$ , and  $T_{\text{VFT}}$  are dependent on the composition of mold flux. The parameter  $A_{\text{VFT}}$  is the value of  $\log \eta$  at infinite temperature, and  $T_{\text{VFT}}$  is the temperature (K) at which viscosity becomes infinite. The parameter  $E_{\text{VFT}}$  corresponds to the pseudo-activation energy associated with viscous flow, and is thought to represent a potential energy barrier obstructing the structural rearrangement of the melt.

The quality of regressions can be measured by the parameter Adj.  $R^2$ , which is a value between 0 and 1. Generally speaking, if it is close to 1, it means that the predicted values are very close to the measured ones. The Adj.  $R^2$  can be written as

$$\bar{R}^2 = 1 - \frac{(1 - R^2)(n - 1)}{n - p - 1}, \quad [2]$$

where  $p$  is the total number of explanatory variables in the model, and  $n$  is the sample size.  $R^2$  is the coefficient of determination that can be calculated as

$$R^2 = 1 - \frac{SS_{\text{res}}}{SS_{\text{tot}}}, \quad [3]$$

where  $SS_{\text{res}}$  is the regression sum of the square measured deviation, and  $SS_{\text{tot}}$  is the total sum of the square of the predicted deviations. They can be written as

Table I. The Chemical Composition of Mold Fluxes with Different Content (Weight Percent)

Samples	SiO <sub>2</sub>	CaO	Al <sub>2</sub> O <sub>3</sub>	(Na <sub>2</sub> O + Li <sub>2</sub> O)	F	MnO	Cr <sub>2</sub> O <sub>3</sub>	B <sub>2</sub> O <sub>3</sub>	$R^*$
1	33.78	32.5	3.51	14.56	12.94	0	0	0	0.96
2	32.21	30.92	3.51	14.56	12.94	1.1	2.1	0	0.96
3	30.68	29.45	3.51	14.56	12.94	1.1	2.1	3	0.96
4	29.27	30.86	3.51	14.56	12.94	1.1	2.1	3	1.05
5	27.94	32.14	3.51	14.56	12.94	1.1	2.1	3	1.15

\*  $R$  is the basicity = CaO/SiO<sub>2</sub>.

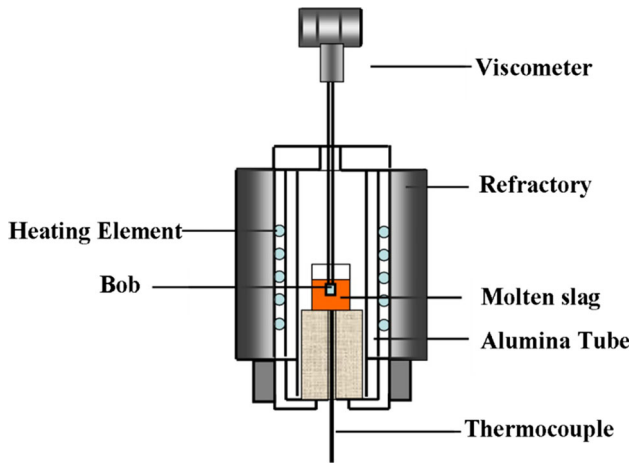


Fig. 1—Schematic figure of viscometer.

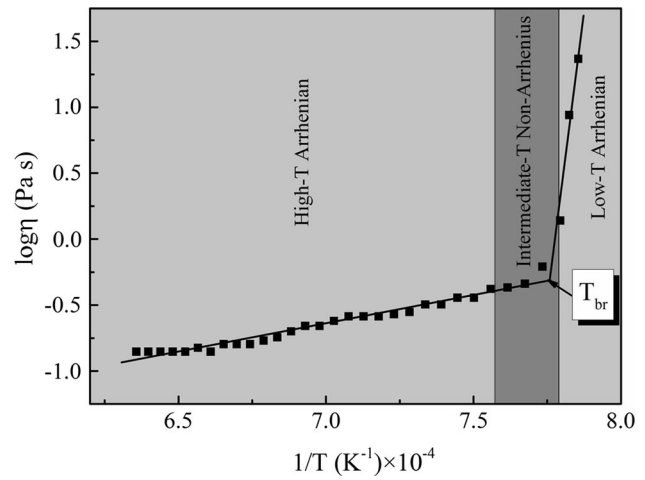


Fig. 2—The variation of viscosity with temperature of Sample 1.

Table II. Dimension and Material of Crucible and Bob

Crucible				Bob		
Graphite	Inner diameter	50 mm	molybdenum	diameter	15 mm	
	Height in total	80 mm	—	height	18 mm	
	Wall thickness	10	—	angle for the tapers	deg	

Table III. The Chemical Composition of Mold Fluxes After the Viscosity Tests (Weight Percent)

Samples	SiO <sub>2</sub>	CaO	Al <sub>2</sub> O <sub>3</sub>	(Na <sub>2</sub> O + Li <sub>2</sub> O)	F	MnO	Cr <sub>2</sub> O <sub>3</sub>	B <sub>2</sub> O <sub>3</sub>	R
1	33.88	32.71	3.72	14.25	12.74	0	0	0	0.96
2	32.35	31.13	3.68	14.24	12.72	1.11	2.12	0	0.96
3	30.79	29.66	3.71	14.22	12.71	1.12	2.12	3.00	0.96
4	29.37	30.92	3.62	14.29	12.81	1.11	2.11	3.01	1.05
5	27.99	32.19	3.61	14.35	12.84	1.10	2.10	3.01	1.15

$$SS_{\text{tot}} = \sum_i (y_i - \bar{y})^2, \quad [4]$$

$$SS_{\text{reg}} = \sum_i (f_i - \bar{y})^2, \quad [5]$$

where  $y_i$  is the measured values of  $\log \eta_i$ ,  $f_i$  is the predicted value of  $\log \eta_i$ , and  $\bar{y} = \frac{1}{n} \sum_{i=1}^n y_i$ .

### III. RESULTS AND DISCUSSIONS

#### A. Comparison of the Arrhenius and the Non-Arrhenius VFT Model

Figure 2 shows the variation of viscosity of Sample 1 vs temperature, which is a typical temperature–viscosity curve of  $\log \eta$  vs  $1/T$  for the mold flux in a wide temperature range from 1200 K (927 °C) to 1573 K (1300 °C). According to the suggestion by Tweer,<sup>[25]</sup> the viscosity in Figure 2 can be divided into three zones. The

first one is the high-temperature Arrhenius zone, where the viscosity of Sample 1 increased with temperature slowly and exhibited an Arrhenius behavior. The second one is the intermediate-temperature zone, in which the viscosity departs from the inverse temperature dependence near the break temperature and starts to show non-Arrhenius characteristics. The viscosity in the third zone returns to the Arrhenius behavior again, although the viscosity increased rapidly, which is called low-temperature Arrhenius zone. Due to the different behavior of viscosity in different temperature zone, the overall variation of viscosity with temperature for Sample 1 shows non-Arrhenius behavior in the whole temperature range. Besides, the break temperature of mold flux, at which the viscosity increases rapidly, can also be obtained from the curve of  $\log \eta$  vs  $1/T$ , and it was about 1302 K (1029 °C) for Sample 1 as shown in Figure 2.

The measured values for the viscosity and temperature of mold flux Samples 1 to 5 during the tests were fitted by Arrhenius ( $\log \eta = A_{\text{VFT}} + \frac{E_{\text{VFT}}}{T - T_{\text{VFT}}}$ ) and non-Arrhenius VFT models, and are shown in Figures 3(a) and (b),<sup>[26]</sup> respectively. It can be seen intuitively in Arrhenius model, as shown in Figure 3(a), that the

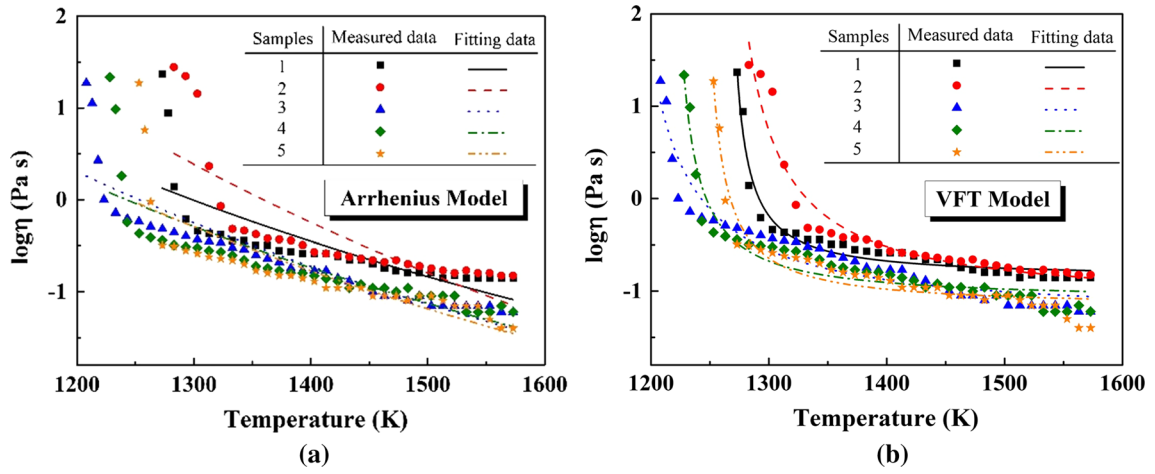


Fig. 3—The fitting of viscosity vs temperature of mold fluxes by using Arrhenius and VFT models. (a) Results from Arrhenius model, (b) Results from VFT model (This figure is being adapted from Ref. [26]).

Table IV. The Adj.  $R^2$  of the Arrhenius and Non-Arrhenius VFT Model

Samples	1	2	3	4	5
Arrhenius Model	0.57	0.62	0.80	0.67	0.65
Non-Arrhenius VFT Model	0.96	0.94	0.92	0.93	0.93

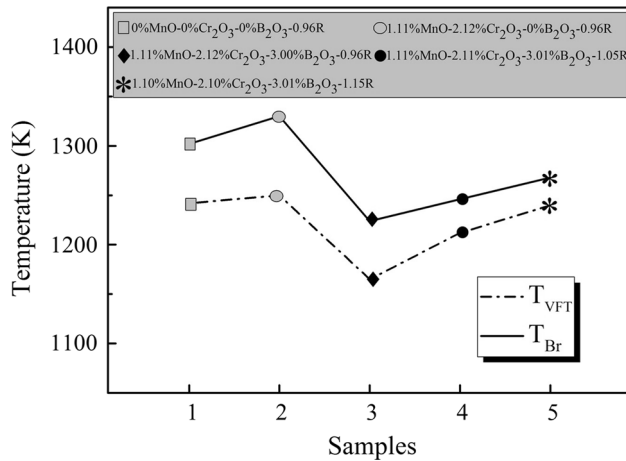


Fig. 4—The  $T_{VFT}$  and  $T_{br}$  temperature of mold fluxes Sample 1 to 5.

deviation between the measured data and the fitting ones is obvious, especially in the low-temperature region, which confirmed that the viscosity of mold flux is not Arrhenius dependent, especially in the low-temperature range. The reason for that is mainly due to the fact that the Arrhenius model is linear related; however, the viscosity of mold flux increases slowly in the high-temperature Arrhenius zone, while it increases sharply in the low-temperature Arrhenius zone, which indicates the relation of  $\log \eta$  vs  $T$  is obviously non-linear related in the whole temperature range. However, the measured data distribute along the fitting line evenly in the VFT model as shown in Figure 3(b), which suggests that the VFT model can be used to well describe the relationship between viscosity and temperature of mold flux.

In order to quantify the quality of linear regression by Arrhenius and VFT models, the adjusted coefficient of determination (Adj.  $R^2$ ) was calculated, and is shown in Table IV. The values for Adj.  $R^2$  of non-Arrhenius VFT Model were from 0.92 to 0.96 that is greatly larger than those of Arrhenius model ranging from 0.57 to 0.80. Therefore, the non-Arrhenius VFT is better for the description of the relationship between viscosity and temperature of mold flux in a wide temperature range.

#### B. Effect of Components on the VFT Temperature of Mold Flux

Through the fitting process of viscosity and temperature using the VFT model, the parameter  $T_{VFT}$  (VFT temperature) can be obtained. According to the Eq. [1], the  $T_{VFT}$  presents the temperature (K) at which viscosity becomes infinite. So, the  $T_{VFT}$  can be considered as another key benchmark to characterize the lubrication ability of mold flux besides the break temperature ( $T_{br}$ ) and glass transition temperature ( $T_g$ ), as all of them indicate that the mold flux loses flowability when the temperature becomes low. The  $T_{VFT}$  and  $T_{br}$  for mold flux Samples 1 to 5 are shown in Figure 4, where the  $T_{VFT}$  of Samples 1 to 5 are 1242 K (969 °C), 1250 K (977 °C), 1165 K (892 °C), 1212 K (939 °C), and 1240 K (967 °C), while the  $T_{br}$  are 1302 K (1029 °C), 1330 K (1057 °C), 1224 K (951 °C), 1246 K (973 °C), and 1268 K (995 °C), respectively. It can be found that the  $T_{br}$  of mold flux are apparently higher than  $T_{VFT}$ . The main reason is that the break temperature is obtained at the temperature where the viscosity of mold flux starts to increase rapidly, but the VFT temperature is corresponding to the temperature at which the

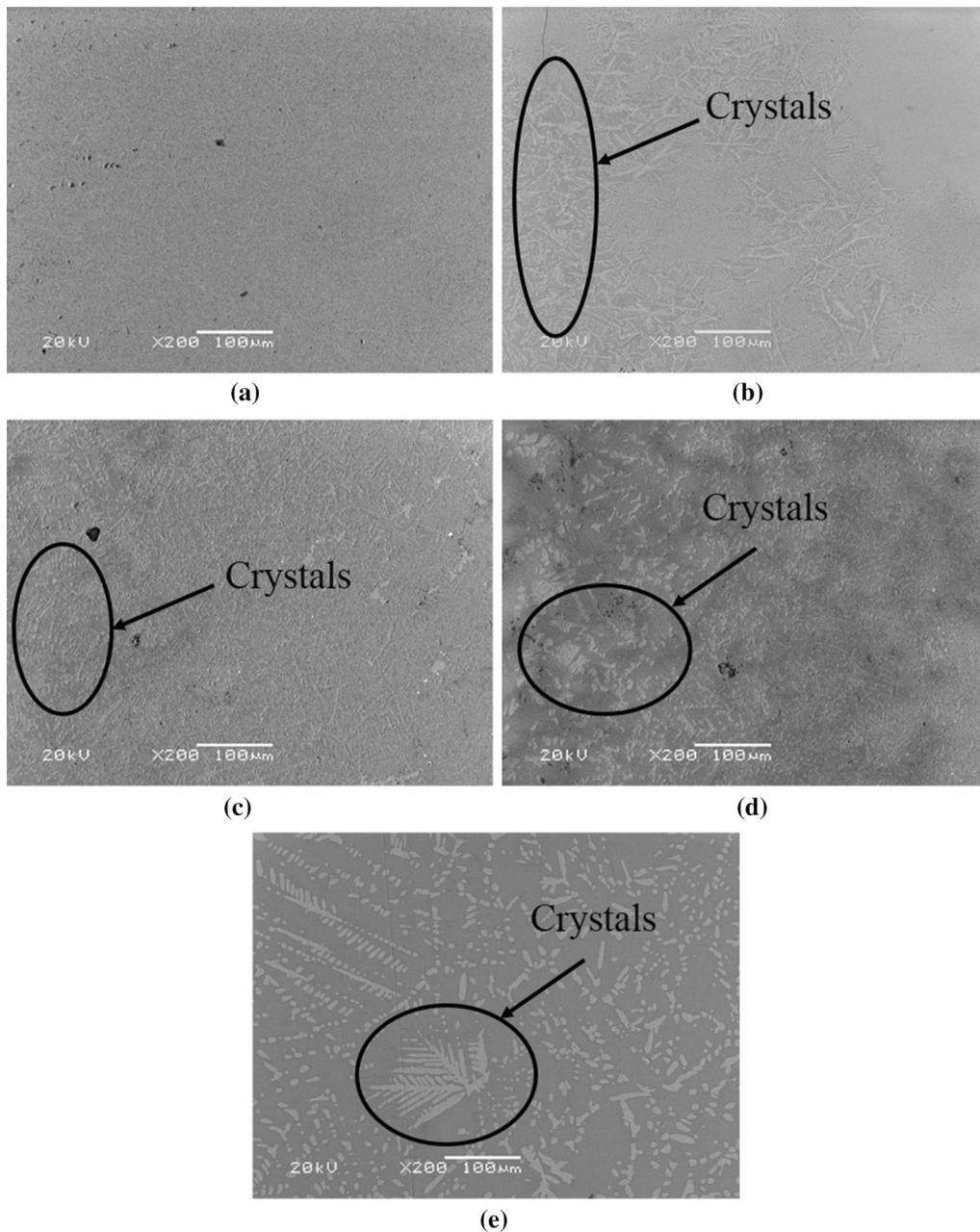


Fig. 5—SEM of mold flux samples after viscosity test. (a) Sample 1, (b) Sample 2, (c) Sample 3, (d) Sample 4, and (e) Sample 5.

viscosity becomes infinite. Besides, the viscosity of mold flux always increases with the reduction in temperature. So, the  $T_{VFT}$  should be lower than  $T_{br}$ . Although the variation trend of  $T_{VFT}$  and  $T_{br}$  is consistent with each other as shown in Figure 4, it is convenient to use the  $T_{VFT}$  to describe mold flux lubrication ability, as it can be calculated directly and accurately from the VFT models based on the viscosity and temperature data from the measurements; however, it may introduce errors when obtaining  $T_{br}$  due to the arbitrary estimation on the slope of viscosity–temperature curve.

Besides, the VFT temperature of Samples 1 to 5 is different from each other, which suggests that the  $T_{VFT}$  of mold flux is dependent on its individual chemical composition. Comparing Sample 1 with Sample 2, the

$T_{VFT}$  increased from 1242 K (969 °C) to 1250 K (977 °C), which attributes to the addition of 1.1 pct MnO and 2.1 pct  $Cr_2O_3$  in the mold flux Sample 2. Although MnO is considered to be a network modifier in molten slag system to lower the degree of polymerization of the melt, the  $Cr_2O_3$  would expect to behave as a network former and increase the viscosity of the mold flux greatly according to our previous paper.<sup>[27]</sup> Thus, the temperature for the viscosity to become infinity would be improved and lead to the increase of  $T_{VFT}$ . The  $T_{VFT}$  of Sample 3 decreased a lot, from 1250 K (977 °C) of Sample 2 to 1165 K (892 °C), with the further addition of 3 pct  $B_2O_3$ . It is resulted from that the  $B_2O_3$  is a typical effective fluxing agent with a low melting point,<sup>[28,29]</sup> which can lower the melting

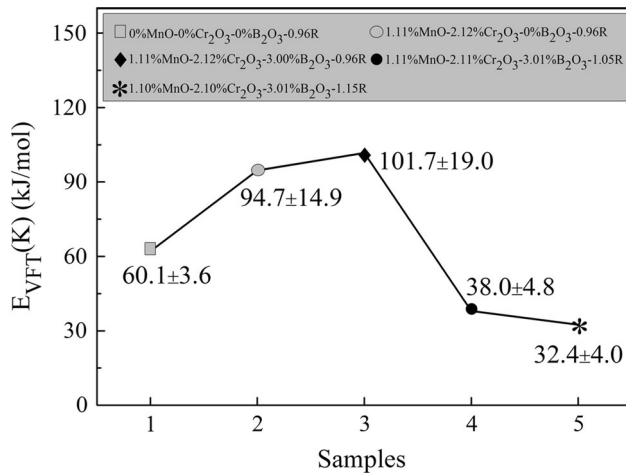


Fig. 6—The pseudo-activation energy  $E_{VFT}$  of mold fluxes.

temperature of mold flux system greatly through the formation of low melting point substances with other components. For Samples 4 and 5, the  $T_{VFT}$  increases continuously to 1212 K (939 °C) and 1240 K (967 °C), respectively, as the basicity (R) is improved from 0.96 to 1.05 and 1.15, which leads to the enhancement of crystallization of mold flux.<sup>[23,24]</sup> Thus, the precipitation temperature of crystal would be high, then the  $T_{VFT}$  of mold flux increased. The SEM photos of the above 5 mold flux samples after the viscosity testes are shown in Figure 5, where the crystals are formed and become very obvious especially in the Samples 4 and 5, which suggests the  $T_{VFT}$  is also affected by the crystallization of mold flux.

### C. Effect of Components on the Pseudo-activation Energy of Mold Flux

The parameter  $E_{VFT}$  in Eq. [1] is the pseudo-activation energy, representing the energy barrier that the ion clusters should overcome during the transport process in the melt. The  $E_{VFT}$  of the above 5 mold flux samples are calculated and shown in Figure 6. They were 60.1 ± 3.6, 94.7 ± 14.9, 101.7 ± 19.0, 38.0 ± 4.8, and 32.4 ± 4.0 kJ/mol for Sample 1 to 5, respectively. It can be seen from Figure 6 that the  $E_{VFT}$  is also varied with the mold flux composition. It increases from 60.1 ± 3.6 kJ/mol (Sample 1) to 94.7 ± 14.9 kJ/mol (Sample 2), and then to 101.7 ± 19.0 kJ/mol (Sample 3) with the addition of MnO and Cr<sub>2</sub>O<sub>3</sub> in Sample 2, as well as the addition of B<sub>2</sub>O<sub>3</sub> in Sample 3. The main reason is Cr<sub>2</sub>O<sub>3</sub> and B<sub>2</sub>O<sub>3</sub> are network formers, which make the ion clusters in the molten mold flux larger and more complex; thus, the energy barrier for the ion clusters to transport increases. On the contrary, the increase of basicity for Samples 4 and 5 would provide more O<sup>2-</sup> to break the bond of Si-Si, and simplify silicate structure leading the movement of ion clusters in molten mold flux easier; thus, the  $E_{VFT}$  for above samples was reduced.

## IV. CONCLUSIONS

The rheological behavior of mold flux was investigated in this paper using the non-Arrhenius temperature-dependent Vogel-Fulcher-Tammann (VFT) model, and the specific important conclusions were summarized as follows:

- (1) The Adj.  $R^2$  of non-Arrhenius VFT Model ranges from 0.92 to 0.96, while those values for Arrhenius model range from 0.57 to 0.80, which suggests that the non-Arrhenius VFT model is better for the description of the relationship between viscosity and temperature of mold flux in a wide range of temperature.
- (2) The  $T_{VFT}$  of Samples 1 to 5 are 1242 K (969 °C), 1250 K (977 °C), 1165 K (892 °C), 1212 K (939 °C), and 1240 K (967 °C), respectively, which are apparently lower than the  $T_{br}$ . It is convenient to use the  $T_{VFT}$  to describe mold flux lubrication ability, as it can be obtained directly and accurately from the VFT model based on the measured viscosity and temperature data.
- (3) The  $T_{VFT}$  of mold flux increased with the increase of Cr<sub>2</sub>O<sub>3</sub> and basicity, while it decreased with the addition of B<sub>2</sub>O<sub>3</sub>, as it was determined by both the degree of polymerization of the melt structure and crystallization behavior of the melt.
- (4) The  $E_{VFT}$  of the five mold flux samples were 60.1 ± 3.6, 94.7 ± 14.9, 101.7 ± 19.0, 38.0 ± 4.8, and 32.4 ± 4.0 kJ/mol for Sample 1 to 5, respectively. It increased with the addition of Cr<sub>2</sub>O<sub>3</sub> and B<sub>2</sub>O<sub>3</sub>, but decreased with the increase of basicity.

## ACKNOWLEDGMENTS

This work was financially supported by the National Science Foundation of China (51504294, 51322405), and the China Postdoctoral Science Foundation (2016T90760) is also great acknowledged.

## REFERENCES

1. T. Kajitani, Y. Kato, K. Harada, K. Saito, K. Harashima, and W. Yamada: *ISIJ Int.*, 2008, vol. 48, pp. 1215–24.
2. E. Takeuchi and J.K. Brimacombe: *Metall. Trans. B*, 1984, vol. 15, pp. 493–509.
3. Y. Chung and A.W. Cramb: *Metall. Mater. Trans. B*, 2000, vol. 31B, pp. 957–71.
4. B. Thomas and J. Sengupta: *JOM*, 2006, vol. 58, pp. 16–18.
5. H. Harmuth and G. Xia: *ISIJ Int.*, 2015, vol. 55, pp. 775–80.
6. A. Kondratiev, E. Jak, and P.C. Hayes: *JOM*, 2002, vol. 54, pp. 41–45.
7. L. Zhou, W. Wang, and K. Zhou: *ISIJ Int.*, 2015, vol. 55, pp. 1961–24.
8. G. Kim and I.L. Sohn: *Metall. Mater. Trans. B*, 2013, vol. 45B, pp. 86–95.
9. X. Qi, G. Wen, and P. Tang: *J. Iron Steel Res. Int.*, 2010, vol. 17, pp. 6–10.
10. Z. Zhang, G. Wen, P. Tang, and S. Sridhar: *ISIJ Int.*, 2008, vol. 48, pp. 739–46.

11. E. Benavidez, L. Santini, M. Valentini, and E. Brandaleze: 11th International Congress on Metallurgy & Materials SAM/CON-AMET 2011, 2012, vol. 1, pp. 389–96.
12. T. Iida, H. Sakai, Y. Kita, and K. Shigeno: *ISIJ Int.*, 2000, vol. 40, pp. S110–S114.
13. K.C. Mills and S. Sridhar: *Ironmak. Steelmak.*, 1999, vol. 26, pp. 262–68.
14. H.S. Ray and S. Pal: *Ironmak. Steelmak.*, 2004, vol. 31, pp. 125–30.
15. D.H. Vogel: *Physikalische Zeitschrift*, 1921, vol. 22, pp. 645–46.
16. G.S. Fulcher: *J. Am. Ceram. Soc.*, 1925, vol. 8, pp. 339–55.
17. G. Tammann and W. Hesse: *Z. Anorg. Allg. Chem.*, 1926, vol. 156, pp. 245–57.
18. D. Giordano and D.B. Dingwell: *Earth Planet. Sci. Lett.*, 2003, vol. 208, pp. 337–49.
19. D. Giordano, J.K. Russell, and D.B. Dingwell: *Earth Planet. Sci. Lett.*, 2008, vol. 271, pp. 123–34.
20. C.A. Angell: *J. Phys. Chem. Solids*, 1988, vol. 49, pp. 863–71.
21. H. Lu and W. Huang: *Smart Mater. Struct.*, 2013, vol. 22, pp. 1–8.
22. B. Mokhtarani, A. Sharifi, H.R. Mortaheb, M. Mirzaei, M. Mafi, and F. Sadeghian: *J. Chem. Thermodyn.*, 2009, vol. 41, pp. 323–29.
23. L. Zhou, W. Wang, B. Lu, and G. Wen: *Met. Mater. Int.*, 2015, vol. 21, pp. 126–33.
24. L. Zhou, W. Wang, F. Ma, J. Li, J. Wei, H. Matsuura, and F. Tsukihashi: *Metall. Mater. Trans. B*, 2012, vol. 43B, pp. 354–62.
25. H. Tweer, J.H. Simmons, and P.B. Macedo: *J. Chem. Phys.*, 1971, vol. 54, pp. 1952–59.
26. L. Zhou and W. Wang: *Metall. Mater. Trans. B*, 2016, vol. 47B, pp. 1548–52.
27. C. Xu, W. Wang, L. Zhou, S. Xie, and C. Zhang: *Metall. Mater. Trans. B*, 2015, vol. 46B, pp. 882–92.
28. V. De Eisenhüttenleute: *Slag Atlas*, 2nd ed., Verlag Stahleisen GmbH, Dusseldorf, 1995, p. 119.
29. L. Zhou, W. Wang, J. Wei, and K. Zhou: *ISIJ Int.*, 2015, vol. 55, pp. 821–29.